

Evolutionary states and triplicity of four massive semi-detached binaries with long-term decreasing orbital periods in the LMC

FU-XING LI,^{1,2} SHENG-BANG QIAN,^{1,*} LI-YING ZHU,² WEN-PING LIAO,² ER-GANG ZHAO,² MIN-YU LI,² QI-BIN SUN,¹
LIN-FENG CHANG,¹ AND WEN-XU LIN²

¹*Department of Astronomy, School of Physics and Astronomy, Yunnan University, Kunming 650091, PR China*

²*Yunnan Observatories, Chinese Academy of Sciences (CAS), P.O. Box 110, 650216 Kunming, PR China*

ABSTRACT

The massive semi-detached binary with a long-term decreasing orbital period may involve a rapid mass-transfer phase in Case A, and thus they are good astrophysical laboratories for investigating the evolution of massive binary stars. In this work, by using the long-term observational light curves from the OGLE project and other data in the low-metallicity LMC, four semi-detached massive binaries with long-term decreases in the orbital periods are detected from 165 EB-type close binaries. It is found that the more massive component in S07798 is filling its Roche lobe where the period decrease is caused by mass transfer from the primary to the secondary. However, the other three (S03065, S12631, S16873) are semi-detached binaries with a lobe-filling secondary where the mass transfer between the components should cause the period to increase if the angular momentum is conservative. The long-term period decreases in these three systems may be caused by the angular momentum loss. Additionally, the orbital periods of three systems (S03065, S07798, S16873) are detected to show cyclic variation with periods shorter than 11 years, which can be plausibly explained by the presence of close-in third bodies in these massive binaries. Based on all of these results, it is suggested that the detected four semi-detached binaries almost have multiplicity. The companion stars are crucial for the origin and evolution of these massive close binaries.

Keywords: binary(including multiple): close - stars: binaries: eclipsing - stars: evolution - stars: individual (LMC)

1. INTRODUCTION

Massive stars, due to their high luminosity, dramatic evolution, and short evolutionary timescale, significantly influence the luminosity distribution, metallicity distribution, and other critical parameters of celestial systems (Pettini et al. 2000; Nomoto et al. 2013; Kummer et al. 2023). Meanwhile, the massive binary is one of the most important stars, on the one hand, these binaries have a plethora of physical processes and astrophysical phenomena, such as gravitational waves (Abbott et al. 2016), X-ray binaries (Verbunt 1993), gamma-ray bursts (Izzard et al. 2004), etc. On the other hand, they provide an ideal test platform to determine the basic information about the components of binaries, and then provide clues to the formation and evolution that we need to understand about massive stars. Especially, since the metallicity of the Large Magellanic Cloud (LMC) is lower than that of the Milky Way (Choudhury et al. 2016), and massive stars have a weakness of the stellar winds at low metallicity (Yoon & Langer 2005), the study of massive binaries in the LMC may be even more significant.

In the case of massive binaries, the first point of emphasis should be their multiplicity. A study by Sana et al. (2012) indicates that more than 70% of massive stars exchange mass with their companions via Roche lobe overflow. Moe & Di Stefano (2017) and Offner et al. (2023) have compiled observational and theoretical findings on stellar multiplicity, demonstrating that over 35% of OB stars refer to triple or higher-order systems, with this proportion increasing with the component mass of the binary. Kummer et al. (2023) discusses interactions in massive triple stars, and describes

Table 1. The basic information of the four binaries.

Parameters	S03065	S07798	S12631	S16873
Period(days)	1.0801861	0.8004206	1.0702108	1.0793907
Epoch(HJD-2 450 000)	7 000.2805	7 000.0085	7 000.4173	7 000.1451
I (mag)	15.961	17.009	16.071	16.07
V (mag)	15.788	16.937	15.915	15.948
$V - I$ (mag)	-0.173	-0.072	-0.156	-0.122
$E(V - I)$ (mag)	0.068	0.109	0.078	0.077
$(V - I)_0$ (mag)	-0.241	-0.181	-0.234	-0.199
T_{M_v} (K)	21 500	16 600	20 900	17 600
Source	OGLE III+IV, TESS	OGLE III+IV+II	OGLE III+IV, EROS-2, TESS	OGLE III+IV+II, TESS

the evolution of a triple star system when taking into account the dynamics of the third body. Additionally, some results show that tertiary companions can dynamically interact with the binary, causing changes in orbital parameters through mechanisms such as Lidov-Kozai oscillations (Naoz & Fabrycky 2014; Naoz 2016), which suggest that tertiary companions will shed new light on the formation and evolution of massive binaries.

Secondly, the evolution of the majority of massive binaries is also dominated by mass transfer (Wellstein & Langer 1999; Marigo et al. 2017; Cehula & Pejcha 2023). Kummer et al. (2023) shown that there are 65%–77% massive binaries with a companion experiencing a phase of mass transfer, initiating the so-called Case A mass transfer phase, and its donor star is often a main sequence. For instance, Rickard & Pauli (2023) found a massive binary with mass transfer in this phase in the Small Magellanic Cloud. Podsiadlowski (2010) also pointed out that mass transfer occurs during the Case B process, which evolves across the Hertzsprung gap. In this process, massive binaries evolve from a detached state to a semidetached binary system, where the more massive component, fills its Roche lobe, and then the mass transfer occurs on the thermal timescale, leading to a decrease in the orbital period of the binary. However, the thermal timescale is too short, and observational samples of massive binaries are very limited. The observational results suggest that many massive binaries undergo a mass ratio inversion, leading to an increase in orbital period due to mass and angular momentum transfer (Taam & Sandquist 2000; Qian et al. 2007; Sen et al. 2022). For example, TU Mus and V382 Cyg (Qian et al. 2007), BH Cen (Zhao et al. 2018), V Pup (Qian et al. 2008; Budding et al. 2021), etc, represent this class of massive binaries with a long-term increasing orbital period. We also try to find those massive binaries with long-term decreasing orbital periods, but these observational samples are rare, with V606 Cen (Li et al. 2022) and GU Mon (Yang et al. 2019) serving as representatives. Therefore, this study aims to search for these rare massive binaries in the LMC, focusing on semidetached binaries, which provide favourable conditions for studying mass transfer in massive stars. This will provide observational evidence to test theories on the formation and evolution of massive binaries.

Based on the Optical Gravitational Lensing Experiment (OGLE) project, it is an ideal laboratory for providing numerous light curves and long-term continuous observations, Pawlak et al. (2016) discovered 40 204 EBs in the LMC from the fourth phase of the OGLE project, and a large number of semidetached binary candidates can be obtained from the non-contact binaries in this catalog. Moreover, substantial results have been obtained on the period variations in binary systems (Zasche et al. 2017; Hajdu et al. 2019, 2022), which suggest that it is a valuable opportunity to search for the targets of this study. Through detailed studies of semidetached massive binaries with long-term decreasing orbital periods, it has been possible to explore the formation channels and evolutionary paths of massive binaries from the discussion of mass transfer, mass and angular momentum loss, and the influence of third bodies. The outline of the paper is as follows: Section 2 explains the source of the data acquisition and the massive binary systems obtained, Section 3 provides a comprehensive analysis of the changes in orbital periods, Section 4 accomplishes the determination of the physical parameters, and Section 5 offers the discussion and conclusion.

2. DATA AND BINARY SYSTEMS

2.1. Data source

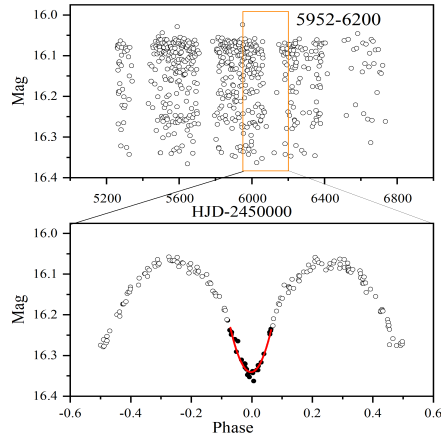


Figure 1. A eclipse time of S12631. The lower panel shows the phase curves obtained from converting 120 data points. A parabolic fit was performed using the data within a phase width of 0.14 to determine the time of the minimum.

The OGLE project is a long-term project with the main goal of searching for the dark matter with microlensing phenomena. However, it has accumulated much valuable data with long-term observations over the past 30 years in specific regions, including light curves of eclipsing binaries in the Magellanic Clouds and the Milky Way. These light curves have stimulated our interest in studying the evolution of massive binaries in the LMC. Therefore, we downloaded all the light curves from the OGLE¹ in the LMC, there are mainly two parts (OGLE III and OGLE IV), and these curves were obtained with the I and V band filters, and took about 90% data in the I band. So, only the I light curves were used to drive the orbital period changes, and those of both bands were used to determine the fundamental parameters for the binaries. As well as using OGLE III and OGLE IV, some datasets and survey data have also been used to extend the time span of the observed targets. These include the OGLE II and EROS-2 surveys², and data from the Transiting Exoplanet Survey Satellite (TESS; Ricker et al. 2015), that have been obtained with high-quality aperture photometry. EROS-2 and OGLE II conducted observations almost simultaneously, which is used when OGLE II is not available. The detailed information is given in Table 1. The OGLE project was equipped with the chip mosaic CCD camera on the 1.3-meter diameter telescope at Las Campanas Observatory, Chile. The EROS-2 survey was carried out with the 1-meter telescope at ESO, La Silla.

TESS is a great all-sky survey that is designed to detect small transiting planets orbiting the brightest and nearest stars in the sky (Stassun et al. 2018). The targets in the LMC have been observed many times in the TESS project, sector 1-13, sector 27-39, and sector 61-69. Since the official did not include light curves for these four targets, the light curves were extracted by applying a new aperture photometry program to the TESScut (Brasseur et al. 2019) fits³, which are available at MAST doi:10.17909/r1b8-aj60. When extracting the light curves, the percentile threshold of background and aperture were set to be 10% and 70%, respectively, only one pixel was selected as the aperture and the detrending was performed using the Something method (Lowess). Despite our efforts to obtain light curve data from all sectors, some sectors were excluded due to poor data quality. As a result, due to the dense star field and the fact that these candidate binaries are not very bright, the TESS light curves have a larger scatter than those of OGLE. We only used sectors with better data quality, and one of the targets was not derived from the TESS light curves. However, the TESS data will be useful for further analysis and study.

2.2. Targets

The aim of this study is to study the evolution of the massive semidetached binaries with long-term orbital period decreases in the LMC. Therefore, several methods have been used to find these binaries, and the detailed information is as follows: (1) Based on the work from Pawlak et al. (2016), which listed the classification (contact and non-contact binaries), and all non-contact binaries were selected. (2) This work focused on the massive binary systems (i.e., spectral type earlier than B5V after considering reddening), we used the criteria with a color index of $V - I$ below 0.0 and

¹ <http://ogle.astrouw.edu.pl/>

² <https://vizier.cds.unistra.fr/viz-bin/VizieR>

³ <https://mast.stsci.edu/tesscut/>

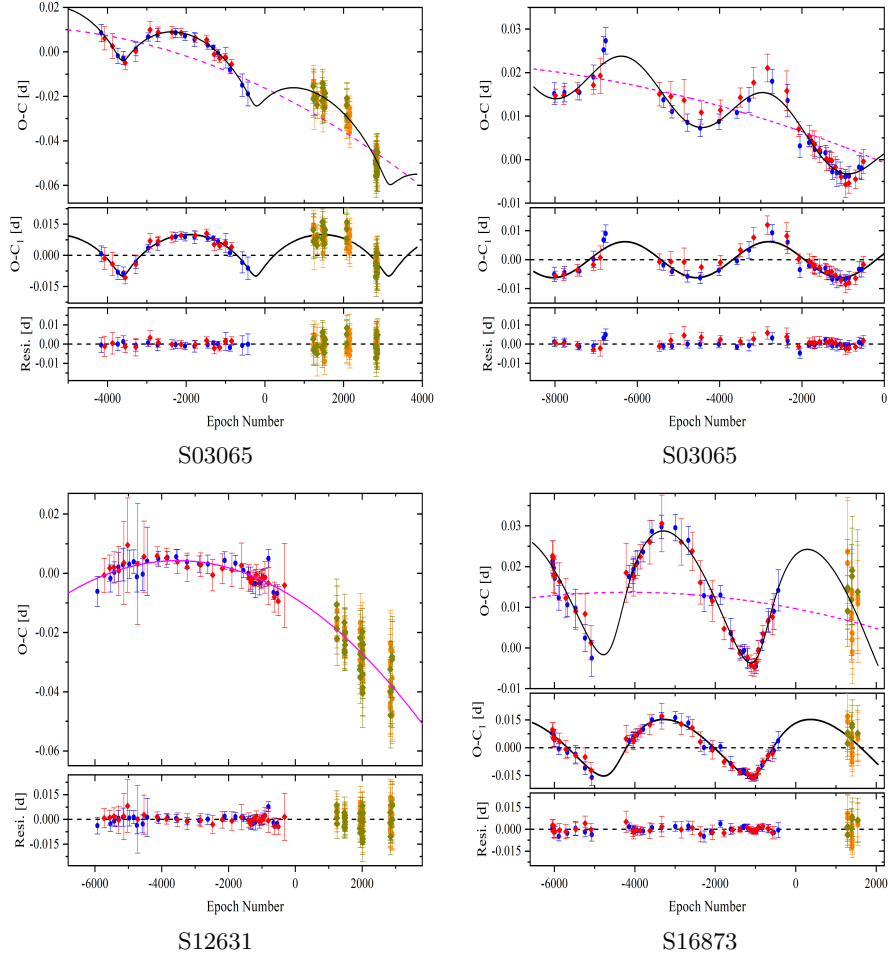


Figure 2. The (O–C) diagrams for four binaries. The upper panels represent the (O–C) curves using all minima (the blue and red dots derived from OGLE or EROS-2, the orange and dark yellow symbols obtained from TESS), while the lines refer to their trends. The middle panels (except for S12631) and lower panels represent the cyclic oscillations and the residuals respectively.

$(V - I)_0$ below -0.165 . The basic information of the binaries were derived from Pawlak et al. (2016), and $E(V - I)$ values were provided by Skowron et al. (2021). These binaries were removed when the eclipse depth was below 0.1 magnitudes for high-quality results, and there were 1178 targets left. (3) We got the binaries with EB-type or EB-like light curves by eyes, and 165 candidates were determined. (4) We created the O-C (observational minima - calculated minima) curves based on the minima of the binaries for these 165 candidates using OGLE III and IV light curves. Then the desired result has been obtained with a downward parabolic trend in the O-C curves, and the trend may imply a long-term decrease in the orbital period and result in about 10 systems being retained. (5) The time series is very important to determine a change of orbital period. So, the data from OGLE II, EROS-2, and TESS were used to identify and test the changes for these massive binaries. Finally, by deriving the light curve solutions, 4 semidetached massive binaries with a long-term decrease in orbital period are identified. The details are given in Table 1. For convenience, all of the systems are referred to as SXXXXX from the initial name of OGLE LMC-ECL-XXXXX in this work.

3. PERIOD VARIATIONS AND LIGHT TRAVEL-TIME EFFECT

3.1. Eclipse times

In binary systems, the time of a minimum (eclipsed by its component) provides valuable information about the system. Analysing the variations of these minima (O-C) based on the theory of light travel-time effect (LTTE), reveals physical phenomena such as changes in magnetic activity or the influence of a third body. For instance, a

periodic change represents the gravitational effect of a third body orbiting the binary system (Li et al. 2022; Leichty et al. 2024). Additionally, mass transfer between components or the loss of mass and angular momentum can lead to parabolic changes in the O-C curve (Qian et al. 2007; Li et al. 2021).

In this study of massive binaries, periodic oscillations in O-C are typically attributed to gravitational perturbations from a third body. For the O-C analysis, more sufficient minima have been used, making the results more accurate. Traditionally, an eclipse timing is obtained from continuous observations during a primary or secondary eclipse. However, with the release of large survey data, a new approach to obtaining minima has been adopted. This method converts discontinuous time series into phases and derives a minimum by shifting the phase over a period, and all the minima in this paper have been derived using survey data by this method. Li et al. (2022) has confirmed the reliability of this approach, which is similar to the method employed by Zasche et al. (2014) and referred to as semi-automatic fitting procedure (APF). This has led to the discovery of many hierarchical triple system candidates in the Galactic Bulge (Hajdu et al. 2019, 2022) and the Small Magellanic Cloud (Zasche et al. 2017).

We employed 120 data points to determine the primary and secondary minima (as illustrated in Figure 1) for OGLE and EROS-2 in this work. Then 50 data points were shifted to determine the subsequent minimum, which can obtain more and denser minima. The continuous light curves obtained from TESS data have a large dispersion, and the minima used in the text are also fitted using the same method with data of multiple periods. The TESS times of minima were originally determined in BJD and then converted to HJD. All the minima of four massive binaries are listed in the table in the appendix.

3.2. Period variation analysis

Based on the minima obtained for four massive binaries, we use the LTTE to perform the O-C calculation. For this step, correct linear ephemerides are required, which are taken from Pawlak et al. (2016) as detailed in Table 1. For these four massive binaries, the time spans range from 16.5 to 25.9 years, and the O-C curves are plotted in the upper panel of Figure 2. In these figures, the O-C values for primary and secondary minima are displayed in different colours, the primary minima for OGLE and EROS-2 are represented in blue, while that for TESS are shown in orange. The primary minima are calculated using the linear ephemerides from Table 1.

The O-C curves indicate that all four targets require fitting with downward parabolas, suggesting a long-term orbital decrease, which precisely aims to identify in such special massive binary systems, with S12631 exhibiting this behaviour prominently. Additionally, three out of the four show periodic oscillations, with only S12631 lacking this characteristic, and the strictly periodic variations exceed two cycles. All four binaries are early-type spectroscopic binaries, the most reasonable explanation involves the presence of a third body orbiting the central binary system, which was created by the LTTE. Although periodic variations may also be caused by magnetic activity and mass motion in late-type binaries.

During the fitting process, S03065 and S168731 were fitted with eccentric orbits, while S07798 was fitted with a circular orbit, it is noted that the least-square fit with weights of the errors was used as described in Equation 1.

$$O - C = \Delta T_0 + \Delta P_0 \times E + \beta \times E^2 + \tau, \quad (1)$$

where E represents the epoch number, β indicates the rate of the linear period change, ΔT_0 and ΔP_0 denote the updated epoch and period respectively, τ is the cyclic modulation term induced by the LTTE, which represents the sinusoidal or eccentric function for these three binaries. The eccentric function can be referenced from Li et al. (2022), which provides detailed mathematical equations. We obtain the periodic modulation of O-C after fitting, which allows us to derive parameters of the third body, such as semi-amplitude, period of the third body, and other related parameters. The corresponding parameters and the revised values are listed in Table 2. Where $f(m)$ denotes the mass function of systems hosting a third body, A and e refer to the semi-amplitude and eccentricity respectively. $M_3 \sin(i_3 = 90^\circ)$ is the lowest mass of the third body, determined from the mass of the binaries. D_{max} is the maximum distance between the third body and the binary, determined using Kepler's third law, the observed orbital period (P_3) and the mass of the binary. It should be noted that due to the temporal smoothing associated with the determination of the minima, we perform a smaller semi-amplitude than the actual one, potentially leading to a slight underestimation of the third body parameters derived from the value of the semi-amplitude.

4. LIGHT-CURVE MODELING

Binaries are important because their light curves can be used to determine some of the basic physical parameters of the two components in a binary system. Initially, tools such as the Wilson and Devinney (W-D) program (Wilson

Table 2. Orbital parameters of the third body or revised period for four massive binaries.

Parameters	S03065	S07798	S12631	S16873
$\Delta T_0(d) \times 10^{-3}$	-16.3(± 1.1)	-0.7(± 1.0)	-8.5(± 0.3)	9.6(± 0.8)
$\Delta P_0(d) \times 10^{-6}$	-8.49(± 0.20)	-3.93(± 0.57)	-7.24(± 0.17)	-1.94(± 0.48)
$\beta \times 10^{-10} (d \text{ cycle}^{-1})$	-6.53(± 0.98)	-1.63(± 0.63)	-10.25(± 0.44)	-2.34(± 0.74)
The semi-amplitude, $A(d) \times 10^{-3}$	10.0(± 0.9)	6.2(± 0.6)	...	16.0(± 0.7)
Orbital period, P_3 (yr)	10.01(± 0.13)	7.64(± 0.13)	...	10.76(± 0.10)
Orbital phase, φ (degrees)	...	20.0(± 5.7)
Longitude of the periastron passage, ω (degrees)	269.7(± 8.8)	315.3(± 8.2)
Periastron passage, T_3 (HJD)	2 459 739.43(± 94.22)	2 460 445.11(± 73.05)
Eccentricity, e	0.69(± 0.11)	0	...	0.42(± 0.04)
Mass function, $f(m)(M_\odot)$	0.052(± 0.010)	0.021(± 0.006)	...	0.213(± 0.027)
Projected semimajor axis, $a_{12} \sin i_3$ (au)	1.73(± 0.16)	1.07(± 0.10)	...	2.91(± 0.12)
Projected masses, $M_3 \sin i_3(M_\odot)$	1.90(± 0.09)	1.19(± 0.03)	...	2.94(± 0.08)
D_{max} (au)	11.23(± 1.77)	8.04(± 1.18)	...	10.81(± 1.20)

Table 3. Photometric solutions for four semidetached massive binaries.

Parameters	S03065		S07798		S12631		S16873	
Mode(Semi-detached)	5		4		5		5	
Case	no L_3	L_3	no L_3	L_3	no L_3	L_3	no L_3	L_3
$q(M_2/M_1)$	0.32 $^{+0.05}_{-0.04}$	0.32 $^{+0.02}_{-0.02}$	0.49 $^{+0.01}_{-0.02}$	0.49 $^{+0.01}_{-0.01}$	0.29 $^{+0.11}_{-0.08}$	0.30 $^{+0.01}_{-0.01}$	0.40 $^{+0.13}_{-0.09}$	0.41 $^{+0.01}_{-0.01}$
i ($^\circ$)	74.70 $^{+1.12}_{-1.13}$	78.00 $^{+1.10}_{-1.10}$	82.21 $^{+0.54}_{-0.51}$	84.41 $^{+0.42}_{-0.42}$	66.70 $^{+1.77}_{-1.40}$	67.26 $^{+0.66}_{-0.66}$	64.86 $^{+1.04}_{-0.81}$	67.80 $^{+0.33}_{-0.33}$
T_2 (K)	14212 $^{+168}_{-157}$	14018 $^{+163}_{-163}$	11172 $^{+79}_{-82}$	10804 $^{+75}_{-75}$	15504 $^{+299}_{-271}$	15508 $^{+115}_{-115}$	13178 $^{+234}_{-231}$	12962 $^{+74}_{-74}$
$r_{1,2}$	0.43 $^{+0.01}_{-0.01}$	0.435 $^{+0.003}_{-0.003}$	0.27 $^{+0.01}_{-0.01}$	0.277 $^{+0.004}_{-0.004}$	0.46 $^{+0.03}_{-0.03}$	0.461 $^{+0.002}_{-0.002}$	0.42 $^{+0.02}_{-0.03}$	0.433 $^{+0.008}_{-0.008}$
$\Omega_{1,2}$	2.745 $^{+0.016}_{-0.016}$	2.707 $^{+0.043}_{-0.043}$	3.101 $^{+0.008}_{-0.008}$	3.074 $^{+0.033}_{-0.033}$	2.542 $^{+0.008}_{-0.008}$	2.573 $^{+0.019}_{-0.019}$	2.863 $^{+0.008}_{-0.008}$	2.816 $^{+0.010}_{-0.010}$
$L_1/(L_1 + L_2)$ (V)	0.859 $^{+0.003}_{-0.003}$	0.851 $^{+0.003}_{-0.003}$	0.827 $^{+0.005}_{-0.005}$	0.819 $^{+0.005}_{-0.005}$	0.762 $^{+0.006}_{-0.006}$	0.776 $^{+0.003}_{-0.003}$
$L_1/(L_1 + L_2)$ (I)	0.808 $^{+0.009}_{-0.009}$	0.817 $^{+0.007}_{-0.007}$	0.847 $^{+0.003}_{-0.003}$	0.839 $^{+0.003}_{-0.003}$	0.817 $^{+0.005}_{-0.005}$	0.809 $^{+0.005}_{-0.005}$	0.750 $^{+0.006}_{-0.006}$	0.764 $^{+0.003}_{-0.003}$
$L_3/(L_1 + L_2 + L_3)$ (V%)	2.0 $^{+1.9}_{-1.9}$...	2.8 $^{+3.4}_{-2.8}$...	16.4 $^{+1.4}_{-1.4}$
$L_3/(L_1 + L_2 + L_3)$ (I%)	...	11.3 $^{+3.2}_{-3.2}$...	3.6 $^{+1.8}_{-1.8}$...	5.6 $^{+3.2}_{-3.2}$...	16.8 $^{+1.3}_{-1.3}$
f (%)	70.8 $^{+0.9}_{-0.9}$	74.2 $^{+0.3}_{-0.3}$	61.6 $^{+0.5}_{-0.5}$	65.1 $^{+2.9}_{-2.9}$	86.4 $^{+0.7}_{-0.7}$	85.7 $^{+1.7}_{-1.7}$	77.0 $^{+0.5}_{-0.5}$	84.4 $^{+0.8}_{-0.8}$

Table 4. The timescale for four semidetached massive binaries.

Parameters	S03065	S07798	S12631	S16873
$M_1(M_\odot)$	7.9 $^{+1.6}_{-1.6}$	5.2 $^{+1.0}_{-1.0}$	7.5 $^{+1.5}_{-1.5}$	5.7 $^{+1.1}_{-1.1}$
$L_1(L_\odot)$	3291 $^{+995}_{-995}$	696 $^{+215}_{-215}$	3205 $^{+1320}_{-1320}$	1206 $^{+451}_{-451}$
$\dot{P}(d \text{ yr}^{-1}) \times 10^{-7}$	-4.41 $^{+0.66}_{-0.66}$	-1.49 $^{+0.62}_{-0.62}$	-7.00 $^{+0.30}_{-0.30}$	-1.58 $^{+0.50}_{-0.50}$
$\dot{M}_1(M_\odot)$	-5.06 $^{+1.32}_{-1.32}$	-3.10 $^{+1.42}_{-1.42}$	-6.68 $^{+1.74}_{-1.74}$	-1.85 $^{+0.70}_{-0.70}$
τ (yr) $\times 10^7$	0.50 $^{+0.13}_{-0.13}$	1.48 $^{+0.77}_{-0.77}$	0.33 $^{+0.08}_{-0.08}$	1.23 $^{+0.46}_{-0.46}$
τ_{th} (yr) $\times 10^5$	2.56 $^{+0.78}_{-0.78}$	3.79 $^{+2.01}_{-2.01}$	1.59 $^{+0.80}_{-0.80}$	3.07 $^{+1.31}_{-1.31}$

& Devinney 1971; Wilson 1990; van Hamme & Wilson 2003) were used for this purpose, but now the PHysics Of Eclipsing BinariEs (PHOEBE)⁴ program has attracted more attention. In this work, we modeled the light curves for these binaries using the V, I band data from OGLE IV. With the exception of S03065, only I-band data were observed for this binary. For modeling the light curves of these binary stars, we first used the 2013 version of the W-D program to obtain fundamental parameters and to preliminarily determine the geometric structures of these binaries. Subsequently, to further confirm the results and enhance their reliability, we employed the MCMC method using PHOEBE (2.4.11 script) for modeling and validation (Prša & Zwitter 2005; Ding et al. 2023; Poro et al. 2023). To conserve computational resources, we have used only a portion of the OGLE IV data (within HJD 24 560 000) for the PHOEBE calculation. Although this is partial data, it still covers many periods, and the results of the W-D solution show that the partial data results for these four target stars are almost identical to those obtained using the full OGLE IV data. Similarly, the results of PHOEBE are also similar to those of W-D.

Before light curve modeling, it is necessary to determine some initial parameters that need to be input, such as temperature, gravity-darkening coefficients, and bolometric albedo. These binaries lack spectroscopy, making it difficult to determine accurate temperatures. Based on the basic information provided by Pawlak et al. (2016), the color index $(V - I)_0$ helps to estimate the temperatures of these massive binaries, and the temperatures (T_1) were derived from the online table ⁵ by Mamajek (based mainly on table 5 from Pecaut & Mamajek 2013), their values are shown in Table 1. These binaries belong to the early B-type spectrum, and the effective surface temperatures of star 1 were determined. Consequently, the bolometric albedos $A_1 = A_2 = 1.0$ (Ruciński 1969) and the gravity-darkening coefficients $g_1 = g_2 = 1.0$ (Lucy 1967) were adopted. In W-D, the bandpass limb-darkening coefficients were determined according to the logarithmic function. While it was set as free parameters in PHOEBE, and the model of stellar atmospheres was utilized from Castelli & Kurucz (2004). Additionally, the mass ratio q (M_2/M_1), the orbital inclination i , the effective surface temperature of star 2 (T_2), the equivalent volume radii r_1 or r_2 (relative to semimajor axis), are set as free parameters in PHOEBE, the MCMC approach was used by the Emcee package, the detailed settings included 30 walkers and 2000 iterations for each walker. The distribution of these parameters for these four massive binaries is shown in Figure 3. The process of determining physical parameters in W-D is similar to these references (Li et al. 2022; Wang et al. 2023; Zhang et al. 2023). Confirmation of the geometric structures and some basic physical parameters for these targets, in particular the PHOEBE solution, can help to determine other parameter values. Then, the third section suggests that three of the four binaries have a third body. In the final step, we tried to include the third light and set the mass ratio as a free parameter, which allowed us to perform the final modeling solution of the light curve.

The results of the light curve modeling suggest that these four massive binaries belong to semidetached binaries. Except for S07798, which is the more massive component filling its Roche lobe, the others are the less ones filling their Roche lobes. This distinction is crucial for studying mass transfer in massive binaries, particularly S07798, which may require more attention. The analyses of these light curves are shown in Figure 4. The physical parameters of these four massive binaries are obtained as shown in Table 3. Where for each massive binary system, there are two sets of solutions available, one that includes the third light and one that does not. $f_{1,2}$ and $\Omega_{1,2}$ are the fill ratios and the Roche potentials of star 1 (S03065, S12631, S16873) or star 2 (S07798), respectively, these components that do not fill their Roche lobes, the value of $f_{1,2}$ is the ratio of the corresponding star volume to the Roche lobe volume.

5. DISCUSSION AND CONCLUSIONS

Through created O-C analysis from the minima and derived solution from the light curves in the LMC, this study demonstrates four massive semidetached binaries with a long-term decrease in orbital period. Compared to the number of the massive non-contact binaries (1178) or the massive binaries with EB-type light curves (165), The fraction of massive semidetached binaries showing long-term orbital period decrease is notably small. This rarity adds to their appeal as objects of reliable observational interest. Furthermore, O-C results indicate that three out of the four systems have a third body (75%), forming triple or higher-order multiple systems. This finding is consistent with the results from Li et al. (2023) on the proportion of massive binaries with third bodies in the LMC, which are also notably high. Moe & Di Stefano (2017) and Offner et al. (2023) studies reveal the fraction of the triple systems fraction is about 35% in this mass range, suggesting strong observational results for a high incidence of third bodies in massive binaries.

⁴ <https://phoebe-project.org/>

⁵ http://www.pas.rochester.edu/~emamajek/EEM_dwarf_UBVIJHK_colors_Teff.txt

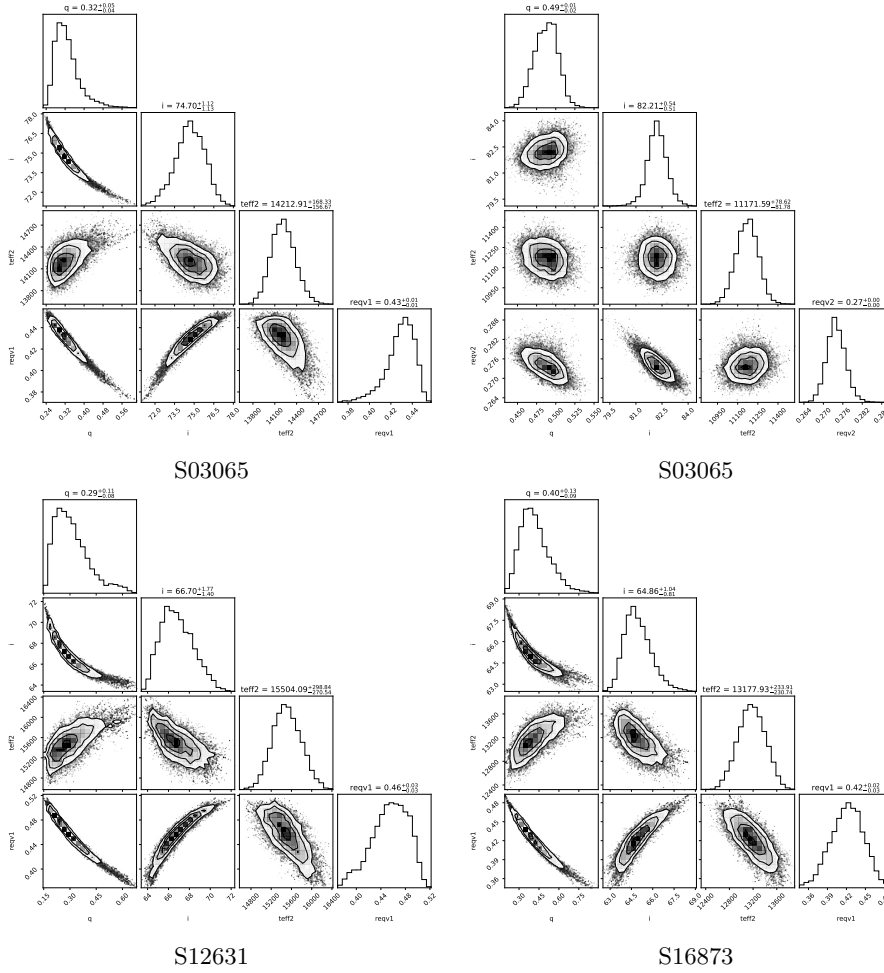


Figure 3. The distribution of the parameters for four massive binaries from the PHOEBE program. q , i , $teff2$, $reqv1$ refer to the mass ratio, orbital inclination, temperature of the secondary star, and the radius of the component that has not filled its Roche lobe, respectively.

This underscores the possibility that the third-body fraction in the LMC might be even higher, potentially influenced by the metallicity of the LMC. It should be noted that the findings may also be influenced by selection effects.

Next, we carried out the third bodies of these massive semidetached binaries to explore the structure of triple systems. The estimates for the third bodies were calculated using Equation 2.

$$f(m) = \frac{(M_3 \sin i)^3}{(M_1 + M_2 + M_3)^2} = \frac{4\pi^2}{GP_3^2} \times (a_{12} \sin i)^3 \quad (2)$$

where $f(m)$ is the mass function of the system, M_1 is shown in Table 4, which is estimated via the color index $(V - I)_0$ by the online table (see also the footnote 5) from Mamajek. The uncertainty is estimated to be 20% of the mass of the primary component. The minimum masses of the third bodies (M_3) were determined to be range between 1.19 and 2.94 M_\odot . Consequently, the minimum mass of the third body of S16873 is larger than that of its secondary component (M_2), which is a B-type spectral companion. This result is consistent with the findings of V357 Cas (Li et al. 2022) and ZZ Cas (Li et al. 2022) from the Milky Way, but the orbital periods of these two binaries are long-term increases, and the third body is much farther away from the central binary, which is very intriguing. In the triple systems S03065 and S07798, the mass of the third body is equal to M_2 only when its orbital inclination is very low. This may imply that these two massive binaries are accompanied by low-mass third bodies, This is similar to the distribution of third bodies in massive binary systems from Li et al. (2023). In these massive binaries with a third body, the results of light curve modeling may also reveal the presence of the third light from the third body. Therefore, these massive binaries

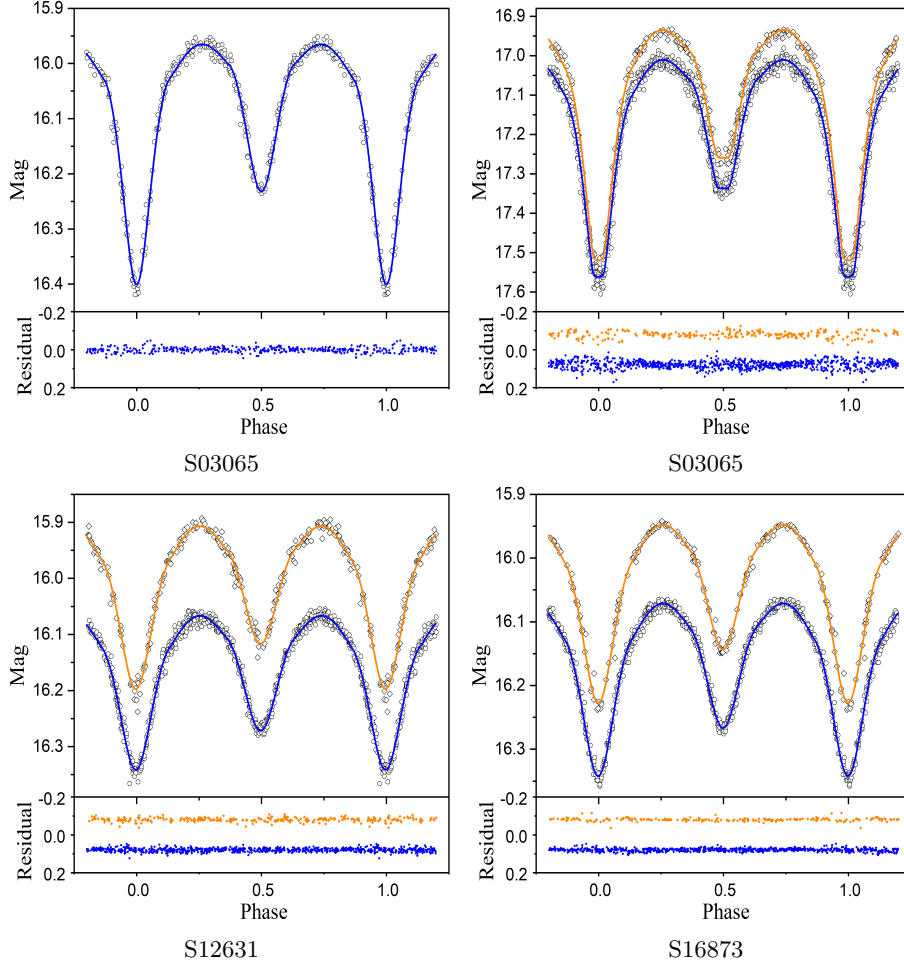


Figure 4. The solid lines (the orange and blue ones refer to the V band and I band, respectively) and black points represent the theoretical and observational light curves for four semidetached binaries in the LMC; Symbols in the lower subpanels in each panel represent the corresponding residual.

and their third components may be forming simultaneously, consistent with the filament fragmentation theory.(Moe & Di Stefano 2017; Moe & Kratter 2018; Tokovinin & Moe 2020; Offner et al. 2023).

Based on the criterion of dynamical stability for the triple system (Mardling & Aarseth 2001; Moe & Kratter 2018; Kummer et al. 2023), they provided the following formula:

$$\left(\frac{a_{\text{out},0}}{a_{\text{in},0}}\right)_{\text{crit}} = \frac{2.8}{1 - e_{\text{out},0}} \left(1 - 0.3 \frac{i_{\text{tot},0}}{180^\circ}\right) \left[\frac{(1 + q_{\text{out}})(1 + e_{\text{out},0})}{\sqrt{1 - e_{\text{out},0}}}\right]^{\frac{2}{5}} \quad (3)$$

where $e_{\text{out},0}$ represents the eccentricity of the third body, $q_{\text{out}} = M_3/(M_1 + M_2)$, and $i_{\text{tot},0}$ is the orbital inclination between the orbits of the inner binary and the outer third body. When $i_{\text{tot},0} = 0$ degrees, based on the minimum mass of the third body in these binaries, the values of $\left(\frac{a_{\text{out},0}}{a_{\text{in},0}}\right)_{\text{crit}}$ for the S03065, S07798, and S16873 systems are 15.1, 3.0, and 7.0, respectively. Whereas the actual $\frac{a_{\text{out}}}{a_{\text{in}}}$ values for these three systems are 38.5, 32.1, and 70.8, respectively. They all belong to hierarchical triple-star systems. Based on this criterion, $\frac{a_{\text{out}}}{a_{\text{in}}} > \left(\frac{a_{\text{out}}}{a_{\text{in}}}\right)_{\text{crit}}$, the actual $\frac{a_{\text{out}}}{a_{\text{in}}}$ values for these three systems are all larger than $\left(\frac{a_{\text{out}}}{a_{\text{in}}}\right)_{\text{crit}}$, indicating that the dynamics of these systems are stable.

We identified four semidetached massive binaries undergoing long-term orbital shrinkage in the LMC. Their rates of orbital variation are on the order of 10^{-7}d yr^{-1} , with periods around one day. However, only the light curve of S07798 supports Mode 4 interpretation, indicating that its more massive component fills its Roche lobe, transferring mass to

the smaller companion, leading to a long-term decrease in orbital period (Sen et al. 2022; Li et al. 2022). In comparison to the thermal timescale, this binary may no longer be in the rapid mass-transfer phase in Case A. Conversely, for S03065, S12631, and S16873, their light curve interpretations suggest these semidetached massive binaries have undergone the stage of mass ratio inversion, the smaller components fill the Roche lobe, transferring mass to their companions, which would normally cause orbital expansion (Qian et al. 2013; Li et al. 2021), contradicting the results exactly. Consequently, which may confirm that these binaries have a significant angular momentum loss, the role it plays is greater than the influence of mass transfer. S03065 and S16873 exhibit the third bodies, likely responsible for angular momentum extraction by the eccentric Kozai-Lidov mechanism (Naoz & Fabrycky 2014; Naoz 2016). Meanwhile, no third body has been detected for S12631, suggesting angular momentum loss may be due to stellar winds or disk winds, gravitational torques, as performed by Kratter (2012) for the angular momentum loss mechanism, and it should also consider the fact that the metallicity of the LMC is lower (Yoon & Langer 2005). Additionally, the mass transfer timescales of the more massive ones were calculated in these binaries by equations 3 (Pringle 1975),

$$\frac{dM_1}{dt} = \frac{M_1 M_2}{3P(M_1 - M_2)} \times \frac{dP}{dt}, \quad (4)$$

the corresponding thermal timescale τ_{th} derived from the following equation 4 (Paczynski 1971),

$$\tau_{\text{th}} = \frac{GM_{1,2}^2}{R_{1,2}L_{1,2}}, \quad (5)$$

and the luminosity of these massive was calculated by the formula as follows,

$$\frac{L_{1,2}}{L_{\odot}} = \left(\frac{R_{1,2}}{R_{\odot}}\right)^2 \times \left(\frac{T_{1,2}}{T_{\odot}}\right)^4. \quad (6)$$

The values are listed in the table 4. The mass-transfer timescales greatly exceed the thermal timescales, both of which relate to the component filling its Roche lobe for these four massive binaries. This evidence may demonstrate that the angular momentum loss dominates the evolution of these massive binaries. However, it should be noted that these findings consider only the currently observed data. Further observations are necessary to explore them.

After that, we try to understand the state of evolution, and the stellar evolutionary tracks and isochrones with a mean metallicity of $[Fe/H] = -0.42$ in the LMC are created based on the CMD 3.7 edition (Bressan et al. 2012; Chen et al. 2014, 2015; Tang et al. 2014; Marigo et al. 2017; Pastorelli et al. 2019), the Hertzsprung-Russell diagram is shown in Figure 5. The results indicate that both the primary and secondary components of these semidetached massive binaries are located in the main sequence.

In summary, there are several aspects of this work are worth consolidating. Firstly, many studies suggest that the proportion of third bodies in massive binaries is very high. These observational results help to confirm this. Importantly, the findings imply that third bodies may play a crucial role in the loss of angular momentum, thereby dominating the influence on the evolution of massive binaries. Secondly, these attractive massive binaries, which have a semidetached geometric configuration with long-term orbital decrease, discover the physical phenomena resulting from the combined effects of mass transfer theories and angular momentum loss mechanisms. It serves as an ideal laboratory to study the mechanism of angular momentum loss in massive systems. These results provide a reasonable explanation for the formation and evolution of massive binary stars.

This work is partly supported by International Cooperation Projects of the National Key R&D Program (No. 2022YFE0127300) and the Chinese Natural Science Foundation (Grant Nos. 12303040, 11933008, 11873017). It is also partly supported by the basic research project of Yunnan Province (Grant Nos. 202401AT070143) and Yunnan Revitalization Talent Support Program. This paper makes use of publicly available data from the OGLE (<https://http://ogle.astrouw.edu.pl/>) and the EROS-2 survey in the VizieR archives (<https://vizier.cds.unistra.fr/viz-bin/VizieR>). All of the TESS data used in this paper can be found through the MAST: [doi:10.17909/r1b8-aj60](https://doi.org/10.17909/r1b8-aj60). The

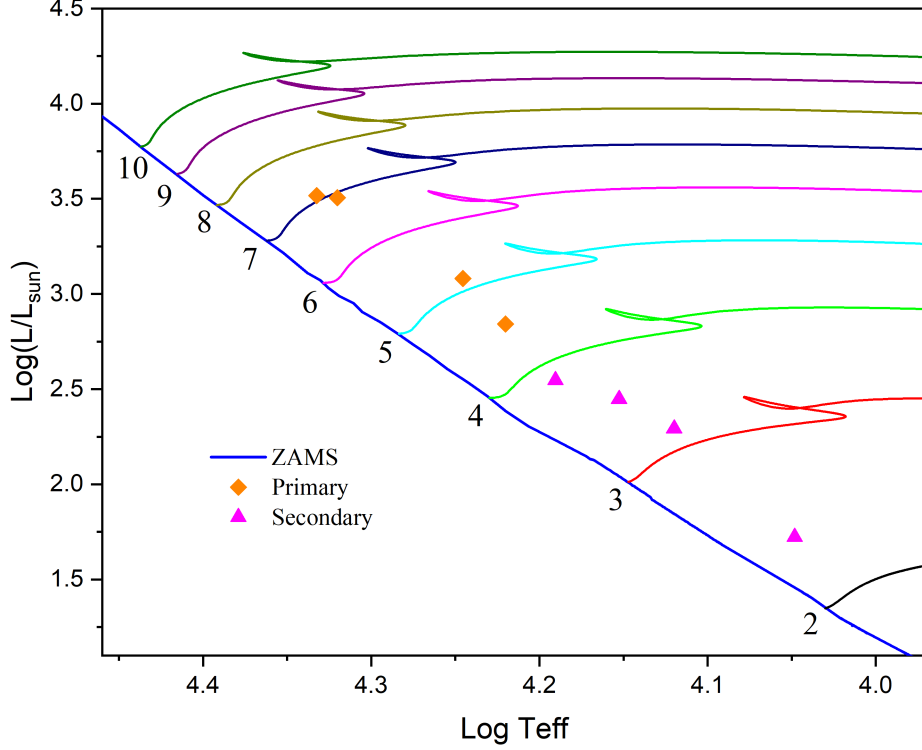


Figure 5. The stellar evolutionary models of four semidetached massive binaries in the LMC. The blue solid line is the ZAMS. The other solid lines represent the evolutionary tracks for the different masses ($2-10M_{\odot}$).

authors thank the OGLE, EROS-2, TESS teams for providing their observation data, which creates an opportunity for us to accomplish this work.

APPENDIX

A. ECLIPSING TIMES TABLE

The eclipse times of the four semidetached massive binaries are shown in Table 5.

Table 5. The eclipsing times of four semidetached massive binaries.

Name	Eclipse-times HJD-2 450 000	Errors \pm days	p/s	Source	Eclipse-times HJD-2 450 000	Errors \pm days	p/s	Source
S03065	2507.79499	0.00383	p	OGLE III	9245.41831	0.00507	s	TESS
	2600.14850	0.00522	s	OGLE III	9245.95394	0.00546	p	TESS
	2815.10209	0.00560	s	OGLE III	9247.58366	0.00704	s	TESS
	2964.70343	0.00342	p	OGLE III	9248.11730	0.00494	p	TESS
	3112.68799	0.00296	p	OGLE III	9249.74722	0.00674	s	TESS
	3163.99461	0.00310	s	OGLE III	9250.27851	0.00493	p	TESS
	3456.73026	0.00451	s	OGLE III	9251.90436	0.00765	s	TESS
	3458.35156	0.00304	p	OGLE III	9252.43981	0.00559	p	TESS
	3795.37504	0.00188	p	OGLE III	9253.52660	0.00837	p	TESS
	3844.52674	0.00365	s	OGLE III	9311.84787	0.00560	p	TESS
	4056.78091	0.00296	p	OGLE III	9312.92819	0.00569	p	TESS
	4071.36473	0.00237	s	OGLE III	9315.08771	0.00685	p	TESS

(Continued)

Table 5. (Continued)

Name	Eclipse-times HJD-2 450 000	Errors \pm days	p/s	Source	Eclipse-times HJD-2 450 000	Errors \pm days	p/s	Source
	4447.26947	0.00262	s	OGLE III	9323.72454	0.00519	p	TESS
	4548.26660	0.00203	p	OGLE III	9324.81564	0.00553	p	TESS
	4696.79210	0.00203	s	OGLE III	9326.97383	0.00527	p	TESS
	4809.67027	0.00199	p	OGLE III	9329.13317	0.00612	p	TESS
	5398.91006	0.00206	s	OGLE IIV	9331.29451	0.00682	p	TESS
	5432.93345	0.00172	p	OGLE IIV	9332.36840	0.00924	p	TESS
	5583.07835	0.00104	p	OGLE IIV	10043.11924	0.00503	p	TESS
	5607.37943	0.00284	s	OGLE IIV	10043.65449	0.00840	s	TESS
	5712.69817	0.00149	p	OGLE IIV	10045.27776	0.00480	p	TESS
	5758.60371	0.00182	s	OGLE IIV	10045.81637	0.00763	s	TESS
	5911.99064	0.00165	s	OGLE IIV	10047.97649	0.00873	s	TESS
	5927.65309	0.00467	p	OGLE IIV	10048.51433	0.00510	p	TESS
	6042.14733	0.00179	p	OGLE IIV	10050.13664	0.00952	s	TESS
	6086.97757	0.00218	s	OGLE IIV	10050.67595	0.00531	p	TESS
	6376.99816	0.00504	p	OGLE IIV	10052.83867	0.00533	p	TESS
	6534.70136	0.00538	p	OGLE IIV	10053.37111	0.00995	s	TESS
	8330.51424	0.00768	s	TESS	10054.99723	0.00532	p	TESS
	8331.05532	0.00561	p	TESS	10057.15578	0.00488	p	TESS
	8336.98989	0.00845	s	TESS	10057.69116	0.00744	s	TESS
	8337.53746	0.00746	p	TESS	10059.86215	0.00732	s	TESS
	8343.47046	0.00713	s	TESS	10060.39806	0.00435	p	TESS
	8344.01306	0.00956	p	TESS	10062.02388	0.00684	s	TESS
	8349.41169	0.01357	p	TESS	10062.56092	0.00436	p	TESS
	8428.80680	0.00580	s	TESS	10064.17798	0.00692	s	TESS
	8429.34767	0.00453	p	TESS	10064.71883	0.00463	p	TESS
	8432.58536	0.00606	p	TESS	10066.33777	0.00961	s	TESS
	8434.20367	0.00599	s	TESS	10066.87995	0.00647	p	TESS
	8575.71002	0.01038	s	TESS	10070.65577	0.00847	s	TESS
	8576.25400	0.00503	p	TESS	10071.20269	0.00676	p	TESS
	8582.72842	0.00648	p	TESS	10073.36760	0.00578	p	TESS
	8583.27917	0.00628	s	TESS	10075.52667	0.00625	p	TESS
	8590.29283	0.00510	p	TESS	10077.68580	0.00667	p	TESS
	8590.83844	0.00707	s	TESS	10078.21862	0.00942	s	TESS
	8593.52561	0.00662	p	TESS	10079.83662	0.00643	p	TESS
	8634.03680	0.00656	s	TESS	10080.37696	0.00843	s	TESS
	8634.58039	0.00356	p	TESS	10084.16143	0.00627	p	TESS
	8641.60296	0.00725	s	TESS	10087.40447	0.00506	p	TESS
	8642.14544	0.00361	p	TESS	10090.63964	0.00612	p	TESS
	8648.08592	0.00339	s	TESS	10093.34832	0.00843	s	TESS
	8648.62102	0.00342	p	TESS	10093.87846	0.00779	p	TESS
	8651.32641	0.00549	s	TESS	10094.96373	0.00999	p	TESS
	8651.86008	0.00577	p	TESS				
S07798	585.45299	0.00249	p	OGLE II	5333.94002	0.00169	s	OGLE IV
	604.26242	0.00150	s	OGLE II	5359.94984	0.00267	p	OGLE IV
	769.14911	0.00208	s	OGLE II	5539.64649	0.00248	s	OGLE IV

(Continued)

Table 5. (Continued)

Name	Eclipse-times HJD-2 450 000	Errors \pm days	p/s	Source	Eclipse-times HJD-2 450 000	Errors \pm days	p/s	Source
	783.15711	0.00216	p	OGLE II	5540.04519	0.00090	p	OGLE IV
	1034.08934	0.00204	s	OGLE II	5588.87117	0.00132	p	OGLE IV
	1072.10897	0.00175	p	OGLE II	5610.08197	0.00280	s	OGLE IV
	1344.65388	0.00205	s	OGLE II	5646.10051	0.00315	s	OGLE IV
	1347.45720	0.00279	p	OGLE II	5648.90084	0.00168	p	OGLE IV
	1479.12669	0.00405	s	OGLE II	5740.54897	0.00296	s	OGLE IV
	1542.76607	0.00309	p	OGLE II	5755.35623	0.00133	p	OGLE IV
	1585.19047	0.00305	p	OGLE II	5857.00945	0.00167	p	OGLE IV
	2628.52646	0.00273	s	OGLE III	5875.01753	0.00267	s	OGLE IV
	2705.76573	0.00173	p	OGLE III	5926.64424	0.00227	p	OGLE IV
	2850.24242	0.00351	s	OGLE III	5939.85131	0.00194	s	OGLE IV
	2872.25049	0.00145	p	OGLE III	5977.47097	0.00189	s	OGLE IV
	3107.97701	0.00480	s	OGLE III	5989.07450	0.00174	p	OGLE IV
	3173.20614	0.00198	p	OGLE III	6049.50726	0.00242	s	OGLE IV
	3421.33523	0.00193	p	OGLE III	6077.92095	0.00312	p	OGLE IV
	3444.15085	0.00271	s	OGLE III	6141.15416	0.00251	p	OGLE IV
	3786.32851	0.00178	p	OGLE III	6160.76354	0.00196	s	OGLE IV
	3812.34486	0.00233	s	OGLE III	6242.80669	0.00162	p	OGLE IV
	4136.11440	0.00129	p	OGLE III	6248.80806	0.00295	s	OGLE IV
	4201.35216	0.00221	s	OGLE III	6311.24116	0.00229	s	OGLE IV
	4370.64055	0.00286	p	OGLE III	6312.44340	0.00232	p	OGLE IV
	4459.89142	0.00354	s	OGLE III	6439.30937	0.00214	s	OGLE IV
	4729.63653	0.00319	s	OGLE III	6510.14935	0.00269	p	OGLE IV
	4819.68079	0.00280	p	OGLE III	6562.17646	0.00261	p	OGLE IV
	5103.42769	0.00458	s	OGLE IV	6592.19378	0.00277	s	OGLE IV
	5119.83409	0.00374	p	OGLE IV				
S12631	658.34198	0.00510	p	EROS-2	8577.88698	0.00603	p	TESS
	877.20553	0.00574	s	EROS-2	8578.41635	0.00608	s	TESS
	1054.86295	0.00443	s	EROS-2	8581.09735	0.00676	p	TESS
	1075.72857	0.00455	p	EROS-2	8581.63369	0.00849	s	TESS
	1189.70975	0.00529	s	EROS-2	8583.77395	0.00808	s	TESS
	1198.80488	0.00350	p	EROS-2	8584.30733	0.00689	p	TESS
	1331.51280	0.00482	p	EROS-2	8586.98485	0.00781	s	TESS
	1342.74876	0.00828	s	EROS-2	8587.51755	0.00563	p	TESS
	1481.34307	0.00548	p	EROS-2	8589.11864	0.00603	s	TESS
	1506.49372	0.01404	s	EROS-2	8589.65822	0.00449	p	TESS
	1627.43347	0.01596	s	EROS-2	8591.79974	0.00556	p	TESS
	1678.26207	0.00480	p	EROS-2	8592.33319	0.00587	s	TESS
	1824.88178	0.00400	p	EROS-2	8592.87054	0.00610	p	TESS
	1925.47649	0.00509	p	EROS-2	8593.40187	0.00602	s	TESS
	1946.34993	0.02050	s	EROS-2	8593.93860	0.00826	p	TESS
	2113.83446	0.00542	p	EROS-2	8594.47655	0.00782	s	TESS
	2149.69247	0.01200	s	EROS-2	9070.17560	0.00809	p	TESS
	2252.96627	0.01150	p	EROS-2	9070.70768	0.00831	s	TESS
	2574.56642	0.00306	s	OGLE III	9073.39134	0.01026	p	TESS

(Continued)

Table 5. (Continued)

Name	Eclipse-times HJD-2 450 000	Errors \pm days	p/s	Source	Eclipse-times HJD-2 450 000	Errors \pm days	p/s	Source
	2610.41754	0.00256	p	OGLE III	9075.52883	0.00797	p	TESS
	2873.15458	0.00323	s	OGLE III	9077.66916	0.00701	p	TESS
	2902.58538	0.00213	p	OGLE III	9078.20978	0.00919	s	TESS
	3187.26180	0.00239	p	OGLE III	9079.81730	0.00760	p	TESS
	3220.97187	0.00410	s	OGLE III	9080.34467	0.00836	s	TESS
	3527.58708	0.00228	p	OGLE III	9081.96061	0.00994	p	TESS
	3533.47147	0.00477	s	OGLE III	9082.47726	0.00878	s	TESS
	3923.56437	0.00273	p	OGLE III	9084.09898	0.00791	p	TESS
	3967.97790	0.00399	s	OGLE III	9084.62157	0.00757	s	TESS
	4196.46811	0.00309	p	OGLE III	9146.15994	0.00702	p	TESS
	4350.03964	0.00531	s	OGLE III	9148.29602	0.00786	p	TESS
	4658.26256	0.00499	s	OGLE III	9148.84578	0.00787	s	TESS
	4737.99600	0.00296	p	OGLE III	9150.44533	0.00789	p	TESS
	4965.41262	0.00569	s	OGLE III	9150.97990	0.00692	s	TESS
	5271.49436	0.00763	s	OGLE IIV	9152.58684	0.00771	p	TESS
	5338.38083	0.00231	p	OGLE IIV	9153.12255	0.00756	s	TESS
	5493.56046	0.00215	p	OGLE IIV	9154.18863	0.00920	s	TESS
	5512.28762	0.00442	s	OGLE IIV	9154.72993	0.01179	p	TESS
	5569.54383	0.00375	p	OGLE IIV	9157.38668	0.01163	s	TESS
	5574.35842	0.00317	s	OGLE IIV	9159.53341	0.00808	s	TESS
	5642.31646	0.00353	p	OGLE IIV	9160.06284	0.00818	p	TESS
	5648.20418	0.00261	s	OGLE IIV	9162.21251	0.00648	p	TESS
	5722.58210	0.00477	p	OGLE IIV	9162.73960	0.00964	s	TESS
	5748.80527	0.00338	s	OGLE IIV	9164.35979	0.00705	p	TESS
	5835.49072	0.00232	s	OGLE IIV	9164.89451	0.00935	s	TESS
	5848.86718	0.00401	p	OGLE IIV	9166.48819	0.00952	p	TESS
	5905.05461	0.00337	s	OGLE IIV	9167.03036	0.00814	s	TESS
	5921.64240	0.00247	p	OGLE IIV	9168.63693	0.00920	p	TESS
	5958.56553	0.00245	s	OGLE IIV	10041.91128	0.00937	p	TESS
	5962.31165	0.00244	p	OGLE IIV	10041.91243	0.01010	p	TESS
	6025.98895	0.00530	s	OGLE IIV	10042.45911	0.00944	s	TESS
	6030.80493	0.00300	p	OGLE IIV	10043.52180	0.01083	s	TESS
	6131.93788	0.00727	s	OGLE IIV	10045.12151	0.00968	p	TESS
	6139.97279	0.00299	p	OGLE IIV	10046.20745	0.01107	p	TESS
	6302.63339	0.00236	p	OGLE IIV	10046.20745	0.01107	p	TESS
	6326.71158	0.00505	s	OGLE IIV	10050.49410	0.01056	p	TESS
	6423.56688	0.00292	p	OGLE IIV	10050.49450	0.01095	p	TESS
	6450.85466	0.00490	s	OGLE IIV	10052.62018	0.01156	p	TESS
	6655.27022	0.01421	s	OGLE IIV	10053.69800	0.01002	p	TESS
	8328.53089	0.00716	p	TESS	10054.21585	0.01102	s	TESS
	8329.07342	0.00862	s	TESS	10054.22369	0.01164	s	TESS
	8330.13909	0.00771	s	TESS	10054.76256	0.01041	p	TESS
	8330.67165	0.00548	p	TESS	10056.89794	0.01000	p	TESS
	8332.81323	0.00559	p	TESS	10056.91368	0.01008	p	TESS
	8333.34611	0.00854	s	TESS	10098.62952	0.00947	p	TESS

(Continued)

Table 5. (Continued)

Name	Eclipse-times HJD-2 450 000	Errors \pm days	p/s	Source	Eclipse-times HJD-2 450 000	Errors \pm days	p/s	Source
	8334.95422	0.00590	p	TESS	10098.63051	0.00972	p	TESS
	8335.48315	0.00894	s	TESS	10099.18358	0.01296	s	TESS
	8336.02746	0.00834	p	TESS	10099.18449	0.01367	s	TESS
	8337.09798	0.00846	p	TESS	10099.71249	0.01231	p	TESS
	8574.14564	0.00961	s	TESS	10101.31429	0.01209	s	TESS
	8574.67891	0.00648	p	TESS	10101.31462	0.01360	s	TESS
	8576.27677	0.00617	s	TESS	10101.84585	0.01393	p	TESS
	8576.81845	0.00625	p	TESS	10102.93228	0.00974	p	TESS
S16873	474.17024	0.00144	p	OGLE II	5507.34678	0.00167	p	OGLE IV
	477.94944	0.00369	s	OGLE II	5571.03077	0.00137	p	OGLE IV
	489.28068	0.00187	p	OGLE II	5618.52439	0.00149	p	OGLE IV
	489.82243	0.00403	s	OGLE II	5702.17555	0.00251	s	OGLE IV
	500.61182	0.00415	s	OGLE II	5711.34996	0.00246	p	OGLE IV
	511.94722	0.00221	p	OGLE II	5799.31867	0.00253	s	OGLE IV
	531.91406	0.00486	s	OGLE II	5803.09651	0.00154	p	OGLE IV
	535.69128	0.00376	p	OGLE II	5881.35189	0.00219	s	OGLE IV
	645.78434	0.00302	p	OGLE II	5884.05034	0.00142	p	OGLE IV
	662.51892	0.00459	s	OGLE II	5932.62321	0.00176	p	OGLE IV
	834.13795	0.00483	s	OGLE II	5934.24327	0.00209	s	OGLE IV
	872.45468	0.00291	p	OGLE II	5996.85072	0.00250	s	OGLE IV
	1094.80831	0.00472	p	OGLE II	5998.47002	0.00232	p	OGLE IV
	1098.58543	0.00449	s	OGLE II	6099.93490	0.00223	p	OGLE IV
	1347.37843	0.00333	p	OGLE II	6116.66728	0.00202	s	OGLE IV
	1349.00346	0.00490	s	OGLE II	6255.91174	0.00244	s	OGLE IV
	1507.66680	0.00420	s	OGLE II	6267.24554	0.00291	p	OGLE IV
	1528.71112	0.00441	p	OGLE II	6373.56640	0.00434	s	OGLE IV
	2449.99211	0.00726	s	OGLE III	6414.04493	0.00436	p	OGLE IV
	2529.32637	0.00274	p	OGLE III	6529.54491	0.00506	p	OGLE IV
	2628.63109	0.00243	p	OGLE III	8388.25559	0.00949	p	TESS
	2632.40846	0.00392	s	OGLE III	8388.79562	0.01223	s	TESS
	2646.98176	0.00265	p	OGLE III	8389.87538	0.00909	s	TESS
	2650.75783	0.00482	s	OGLE III	8390.42113	0.01613	p	TESS
	2707.96841	0.00334	s	OGLE III	8392.58274	0.01267	p	TESS
	2752.76360	0.00303	p	OGLE III	8393.10787	0.00874	s	TESS
	2826.70336	0.00298	s	OGLE III	8492.94966	0.01050	p	TESS
	2903.88098	0.00245	p	OGLE III	8493.49392	0.01368	s	TESS
	3085.76074	0.00537	s	OGLE III	8496.18907	0.01132	p	TESS
	3144.59015	0.00272	p	OGLE III	8497.26820	0.01172	p	TESS
	3400.40688	0.00288	p	OGLE III	8499.43080	0.01127	p	TESS
	3405.26498	0.00697	s	OGLE III	8502.66542	0.01029	p	TESS
	3769.55827	0.00324	p	OGLE III	8505.90916	0.01017	p	TESS
	3926.60614	0.00568	s	OGLE III	8509.14666	0.00775	p	TESS
	4118.19836	0.00343	p	OGLE III	8510.76999	0.01187	s	TESS
	4221.27752	0.00468	s	OGLE III	8511.29412	0.00848	p	TESS
	4439.30678	0.00530	s	OGLE III	8511.85083	0.01324	s	TESS

(Continued)

Table 5. (Continued)

Name	Eclipse-times HJD−2 450 000	Errors ±days	p/s	Source	Eclipse-times HJD−2 450 000	Errors ±days	p/s	Source
	4539.14714	0.00384	p	OGLE III	8512.37044	0.00779	p	TESS
	4730.19891	0.00198	p	OGLE III	8514.53386	0.00873	p	TESS
	4762.04002	0.00496	s	OGLE III	8661.88088	0.01521	s	TESS
	4980.61809	0.00234	p	OGLE III	8663.49891	0.01341	p	TESS
	5256.93270	0.00367	p	OGLE IV	8664.57748	0.00953	p	TESS
	5304.96403	0.00228	s	OGLE IV	8665.65582	0.01444	p	TESS
	5500.33045	0.00170	s	OGLE IV				

REFERENCES

- Abbott, B. P., Abbott, R., Abbott, T. D., et al. 2016, *PhRvL*, 116, 061102. doi:10.1103/PhysRevLett.116.061102
- Brasseur, C. E., Phillip, C., Fleming, S. W., et al. 2019, *Astrophysics Source Code Library*. ascl:1905.007
- Bressan, A., Marigo, P., Girardi, L., et al. 2012, *MNRAS*, 427, 127. doi:10.1111/j.1365-2966.2012.21948.x
- Budding, E., Love, T., Blackford, M. G., et al. 2021, *MNRAS*, 502, 6032. doi:10.1093/mnras/stab381
- Castelli, F. & Kurucz, R. L. 2004, *A&A*, 419, 725. doi:10.1051/0004-6361:20040079
- Cehula, J. & Pejcha, O. 2023, *MNRAS*, 524, 471. doi:10.1093/mnras/stad1862
- Chen, Y., Bressan, A., Girardi, L., et al. 2015, *MNRAS*, 452, 1068. doi:10.1093/mnras/stv1281
- Chen, Y., Girardi, L., Bressan, A., et al. 2014, *MNRAS*, 444, 2525. doi:10.1093/mnras/stu1605
- Choudhury, S., Subramaniam, A., & Cole, A. A. 2016, *MNRAS*, 455, 1855. doi:10.1093/mnras/stv2414
- Ding, X., Ji, K., Li, X., et al. 2023, *MNRAS*, 525, 4596. doi:10.1093/mnras/stad2565
- Hajdu, T., Borkovits, T., Forgács-Dajka, E., et al. 2022, *MNRAS*, 509, 246. doi:10.1093/mnras/stab2931
- Hajdu, T., Borkovits, T., Forgács-Dajka, E., et al. 2019, *MNRAS*, 485, 2562. doi:10.1093/mnras/stz592
- Izzard, R. G., Ramirez-Ruiz, E., & Tout, C. A. 2004, *MNRAS*, 348, 1215. doi:10.1111/j.1365-2966.2004.07436.x
- Kratter, K. M. 2012, *Proceedings of a Scientific Meeting in Honor of Anthony F. J. Moffat*, 465, 451
- Kummer, F., Toonen, S., & de Koter, A. 2023, *A&A*, 678, A60. doi:10.1051/0004-6361/202347179
- Leichty, M., Garnavich, P., Littlefield, C., et al. 2024, *ApJ*, 967, 81. doi:10.3847/1538-4357/ad3bac
- Li, F.-X., Liao, W.-P., Qian, S.-B., et al. 2022, *ApJ*, 924, 30. doi:10.3847/1538-4357/ac3425
- Li, F.-X., Qian, S.-B., Fernández Lajús, E., et al. 2022, *PASJ*, 74, 533. doi:10.1093/pasj/psac016
- Li, F.-X., Qian, S.-B., Zhang, J., et al. 2022, *MNRAS*, 514, 1206. doi:10.1093/mnras/stac1327
- Li, F.-X., Qian, S.-B., Wu, C.-Q., et al. 2023, *ApJ*, 956, 49. doi:10.3847/1538-4357/acf196
- Li, K., Gao, X., Liu, X.-Y., et al. 2022, *AJ*, 164, 202. doi:10.3847/1538-3881/ac8ff2
- Li, K., Xia, Q.-Q., Kim, C.-H., et al. 2021, *AJ*, 162, 13. doi:10.3847/1538-3881/abfc53
- Lucy, L. B. 1967, *ZA*, 65, 89
- Mardling, R. A. & Aarseth, S. J. 2001, *MNRAS*, 321, 398. doi:10.1046/j.1365-8711.2001.03974.x
- Marigo, P., Girardi, L., Bressan, A., et al. 2017, *ApJ*, 835, 77. doi:10.3847/1538-4357/835/1/77
- Moe, M. & Di Stefano, R. 2017, *ApJS*, 230, 15. doi:10.3847/1538-4365/aa6fb6
- Moe, M. & Kratter, K. M. 2018, *ApJ*, 854, 44. doi:10.3847/1538-4357/aaa6d2
- Naoz, S. 2016, *ARA&A*, 54, 441. doi:10.1146/annurev-astro-081915-023315
- Naoz, S. & Fabrycky, D. C. 2014, *ApJ*, 793, 137. doi:10.1088/0004-637X/793/2/137
- Nomoto, K., Kobayashi, C., & Tominaga, N. 2013, *ARA&A*, 51, 457. doi:10.1146/annurev-astro-082812-140956
- Offner, S. S. R., Moe, M., Kratter, K. M., et al. 2023, *Protostars and Planets VII*, 534, 275. doi:10.48550/arXiv.2203.10066
- Paczyński, B. 1971, *ARA&A*, 9, 183. doi:10.1146/annurev.aa.09.090171.001151

- Pastorelli, G., Marigo, P., Girardi, L., et al. 2019, *MNRAS*, 485, 5666. doi:10.1093/mnras/stz725
- Pawlak, M., Soszyński, I., Udalski, A., et al. 2016, *AcA*, 66, 421. doi:10.48550/arXiv.1612.06394
- Pecaut, M. J. & Mamajek, E. E. 2013, *ApJS*, 208, 9. doi:10.1088/0067-0049/208/1/9
- Pettini, M., Steidel, C. C., Adelberger, K. L., et al. 2000, *ApJ*, 528, 96. doi:10.1086/308176
- Podsiadlowski, P. 2010, *NewAR*, 54, 39. doi:10.1016/j.newar.2010.09.023
- Poró, A., Fernández-Lajús, E., Madani, M., et al. 2023, *Research in Astronomy and Astrophysics*, 23, 095011. doi:10.1088/1674-4527/ace027
- Pringle, J. E. 1975, *MNRAS*, 170, 633. doi:10.1093/mnras/170.3.633
- Prša, A. & Zwitter, T. 2005, *ApJ*, 628, 426. doi:10.1086/430591
- Qian, S.-B., Liao, W.-P., & Fernández Lajús, E. 2008, *ApJ*, 687, 466. doi:10.1086/591515
- Qian, S.-B., Yuan, J.-Z., Liu, L., et al. 2007, *MNRAS*, 380, 1599. doi:10.1111/j.1365-2966.2007.12184.x
- Qian, S.-B., Zhang, J., Wang, J.-J., et al. 2013, *ApJS*, 207, 22. doi:10.1088/0067-0049/207/2/22
- Rickard, M. J. & Pauli, D. 2023, *A&A*, 674, A56. doi:10.1051/0004-6361/202346055
- Ricker, G. R., Winn, J. N., Vanderspek, R., et al. 2015, *Journal of Astronomical Telescopes, Instruments, and Systems*, 1, 014003. doi:10.1117/1.JATIS.1.1.014003
- Ruciński, S. M. 1969, *AcA*, 19, 245
- Sana, H., de Mink, S. E., de Koter, A., et al. 2012, *Science*, 337, 444. doi:10.1126/science.1223344
- Sen, K., Langer, N., Marchant, P., et al. 2022, *A&A*, 659, A98. doi:10.1051/0004-6361/202142574
- Skowron, D. M., Skowron, J., Udalski, A., et al. 2021, *ApJS*, 252, 23. doi:10.3847/1538-4365/abcb81
- Stassun, K. G., Oelkers, R. J., Pepper, J., et al. 2018, *AJ*, 156, 102. doi:10.3847/1538-3881/aad050
- Taam, R. E. & Sandquist, E. L. 2000, *ARA&A*, 38, 113. doi:10.1146/annurev.astro.38.1.113
- Tang, J., Bressan, A., Rosenfield, P., et al. 2014, *MNRAS*, 445, 4287. doi:10.1093/mnras/stu2029
- Tokovinin, A. & Moe, M. 2020, *MNRAS*, 491, 5158. doi:10.1093/mnras/stz3299
- van Hamme, W. & Wilson, R. E. 2003, *GAIA Spectroscopy: Science and Technology*, 298, 323
- Verbunt, F. 1993, *ARA&A*, 31, 93. doi:10.1146/annurev.aa.31.090193.000521
- Wang, Z., Zhu, L., & Yuan, K. 2023, *Research in Astronomy and Astrophysics*, 23, 015003. doi:10.1088/1674-4527/ac9f08
- Wellstein, S. & Langer, N. 1999, *A&A*, 350, 148. doi:10.48550/arXiv.astro-ph/9904256
- Wilson, R. E. 1990, *ApJ*, 356, 613. doi:10.1086/168867
- Wilson, R. E. & Devinney, E. J. 1971, *ApJ*, 166, 605. doi:10.1086/150986
- Yang, Y., Yuan, H., & Dai, H. 2019, *AJ*, 157, 111. doi:10.3847/1538-3881/aafef1
- Yoon, S.-C. & Langer, N. 2005, *A&A*, 443, 643. doi:10.1051/0004-6361:20054030
- Zasche, P., Wolf, M., & Vraštil, J. 2017, *MNRAS*, 472, 2241. doi:10.1093/mnras/stx2026
- Zasche, P., Wolf, M., Vraštil, J., et al. 2014, *A&A*, 572, A71. doi:10.1051/0004-6361/201424273
- Zhang, B., Mei, K.-Y., Zhi, Q.-J., et al. 2023, *NewA*, 102, 102038. doi:10.1016/j.newast.2023.102038
- Zhao, E.-G., Qian, S.-B., Zejda, M., et al. 2018, *Research in Astronomy and Astrophysics*, 18, 059. doi:10.1088/1674-4527/18/5/59